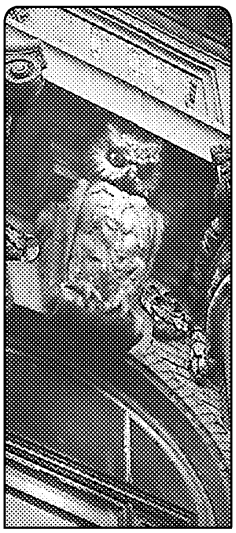

НАУЧНЫЙ ОТДЕЛ

ТЕОРЕТИЧЕСКАЯ И МАТЕМАТИЧЕСКАЯ ФИЗИКА

Известия Саратовского университета. Новая серия. Серия: Физика. 2025. Т. 25, вып. 3. С. 266–276
Izvestiya of Saratov University. Physics, 2025, vol. 25, iss. 3, pp. 266–276
https://fizika.sgu.ru https://doi.org/10.18500/1817-3020-2025-25-3-266-276, EDN: AYKMGN

Review

Maximal field emission current densities in nanostructures

M. V. Davidovich

Saratov State University, 83 Astrakhanskaya St., Saratov 410012, Russia

Michael V. Davidovich, davidovichmv@sgu.ru, https://orcid.org/0000-0001-8706-8523

Abstract. ***Background and Objectives***: The problems of issues of achieving high field emission current densities 2–4 orders of magnitude lower than the limit values 10^{15}-10^{16} A/m^2 are considered. ***Materials and Methods:*** Methods of obtaining them, field emission models, as well as possible emission structures providing large integrated currents in ribbon electron beams are analyzed. ***Results:*** It has been shown that the high current densities of the order 10^{10}–10^{12} A/m^2 can be achieved in vacuum quantum structures with two or more potential wells during resonant tunneling. ***Conclusions:*** Obtaining high-precision sources requires nanotechnology to create heterostructures of the metal-isolator-metal type and the use of low temperatures. Amorphous glass-like diamond (GLD) is a good material for dielectric films, and conductive glass-like carbon (GLC) is a suitable material for conductive films. In fact, the technology of creating thin-film structures such as GLD-GLC-CLD is used.

Keywords: field emission, autocathode, Schrödinger equation, resonant tunneling, Poisson equation

Acknowledgements: This work was supported by the Russian Science Foundation (project No. 21-19-00226) and the Ministry of Science and Higher Education of the Russian Federation within the framework of the State Assignment (no. FSR-2023-0008).

For citation: Davidovich M. V. Maximal field emission current densities in nanostructures. *Izvestiya of Saratov University. Physics*, 2025, vol. 25, iss. 3, pp. 266–276. https://doi.org/10.18500/1817-3020-2025-25-3-266-276, EDN: AYKMGN

Обзор
УДК 535.538.935

Предельно большие плотности тока полевой эмиссии в наноструктурах

М. В. Давидович

Саратовский национальный исследовательский государственный университет имени Н. Г. Чернышевского, Россия, 410012, г. Саратов, ул. Астраханская, д. 83

Давидович Михаил Владимирович, доктор физико-математических наук, профессор кафедры радиотехники и электродинамики, https://orcid.org/0000-0001-8706-8523

Аннотация. Рассматриваются вопросы достижимости высоких плотностей тока полевой эмиссии лишь на 2–4 порядка меньших предельных значений 10^{15}–10^{16} А/м^2. Анализируются способы достижения таких токов, модели полевой эмиссии, а также эмиссионные структуры, обеспечивающие большие интегральные токи в ленточных электронных пучках. Показана достижимость больших значений плотностей тока порядка 10^{10}–10^{12} А/м^{2}в вакуумных квантовых структурах с двумя и более потенциальными ямами при резонансном туннелировании. Получение высокоточных источников сопряжено с созданием гетероструктур типа диэлектрик-проводник-диэлектрик-проводник и использованем низких температур.

Хорошим материалом для диэлектрических пленок является аморфный алмаз (GLD), а для проводящих пленок – проводящий стеклоуглерод (GLC). Наиболее подходящей является CVD технология создания тонкопленочных структур типа GLD-GLC-CLD.

Ключевые слова: полевая эмиссия, автокатод, уравнение Шредингера, резонансное туннелирование, уравнение Пуассона

Благодарности: Работа выполнена при финансовой поддержке Российского научного фонда (проект № 21-19-00226) и Министерства науки и высшего образования РФ в рамках государственного задания (№ FSR-2023-0008).

Для цитирования: Davidovich M. V. Maximal field emission current densities in nanostructures [*Давидович М. В.* Предельно большие плотности тока полевой эмиссии в наноструктурах] // Известия Саратовского университета. Новая серия. Серия: Физика. 2025. Т. 25, вып. 3. С. 266–276. https://doi.org/10.18500/1817-3020-2025-25-3-266-276, EDN: AYKMGN

Introduction. Simple models of one-dimensional tunneling

Field emission (FE) has been known for more than a hundred years and for single cathode in strong electric field was explained by Fowler and Nordheim [1]. It is associated with the emergence of a potential barrier that narrows and decreases in strong fields, as well as with the quantum nature of tunneling electrons. The current density of cold FE is defined as integration of $dJ^+ = e\,j_0 D^+(\mathrm{E})(\mathrm{E}_F - \mathrm{E})d\mathrm{E}$ [2,3] over the energy. Here $j_0 = m_e/(2\pi^2 h^3)$, $D^+(\mathrm{E})$ is the tunneling coefficient from cathode to anode (transparency) for the kinetic energy $\mathrm{E}_k = \mathrm{E}$, M_e is the mass of the electron. It is assumed that the emission occurs at zero temperature from a flat metal cathode. With decreases in kinetic energies significantly below the Fermi energy E_{Fc} at the cathode, this coefficient becomes exponentially small. The result is obtained taking into account the electron velocity distribution at $T = 0$, while $dn_{v_x} = j_0 v_x (v_F^2 - v_x^2) dv_x$ with $\mathrm{E}_k = m_e v_x^2/2$. Assuming that $D^+(\mathrm{E}) = 1$ for all energies (all running electrons pass the barrier), from (1) we get $J^+_{\max} = e\,j_0 \mathrm{E}_F^2/2$ [2, 3]. Taking $\mathrm{E}_F = 7$ eV for copper, we find $J^+_{\max} = 4 \cdot 10^{15}$ A/m^2. For beryllium Be we have $J^+_{\max} = 1.7 \cdot 10^{16}$ A/m^2. This gigantic current density, of course, is not achievable, because the barrier cannot be transparent for all energies. However, for a complex barrier profile with two or more peaks during resonant tunneling (RT), it can be completely transparent for some energies. Further, by the barrier we mean any distribution of the quantum potential $V(x)$ in the region of tunneling. It is tempting to get densities at least 2–4 orders of magnitude lower than the specified limit, i.e. about 10^{11}–10^{13} A/m^2. Are they achievable? In this review, we give an answer to this question, and also consider high-current structures with FE.

The disadvantage of FE cathodes among device developers is considered to be a low current density compared to thermal cathodes, for which the characteristic values are $J \sim 10^6$–10^7 A/m^2. Although operating current densities of FE are actually claimed in pulse modes up to 10^{11} A/m^2 [2, 3]. The FE cathodes and electron guns used in devices with acceptable service lives give densities 4–5 orders of magnitude lower than indicated, i.e. 8–10 orders of magnitude lower than the limit. This is due not to the impossibility of achieving high currents, but mainly to the instability and short duration of high-current cathodes (very high densities of FE and explosive emission were achieved in laboratory conditions in pulsed modes [2, 3]). The main reason for this is the high voltages required for significant FE, the associated reverse ion bombardment of cathodes and explosive FE. To obtain strong fields, pointed cathodes with a relatively small percentage of the emitting surface are used. This is what leads to instability. As a result, the practical majority of vacuum electronic devices use incandescent cathodes and electron guns with thermionic emission. Therefore, the main task of vacuum electronics is to obtain stable high-current sources of FE at relatively low voltages. This is achieved in resonant tunneling nanostructures.

The current state of this problem is considered in the review [4]. For the needs of modern micro- and nano-electronics, in particular, for the TWT millimeter and subterahertz ranges, miniature high-current field sources with thin ribbon relativistic electron beams are needed, providing the beam current from mA and above [4].

The purpose of the review is to clarify of the question of the maximum achievable densities in field vacuum emitting structures. Most of the initial works on FE were based on the Fowler-Nordheim (FN) formula [2–6]. It relates the emission current density to the output work function W for the cathode metal sample and the intensity of the normal component of the electric field at the cathode in the form $J(E_x, W) = AW^{-1}E_x^2 \exp\left(-BW^{3/2}/E_x\right)$. This formula gives an unlimited current density if the field strength increases indefinitely. The formula works for emission from metal cathodes with a flat surface, when the anode is far away with not too strong fields and not too large J. The description of the differences between experiments and FN formula can be found in many works, for example, in [3, 6]. The FN formula does not work for semiconductor cathodes [2], cathodes

with an oxide or dielectric film [2], with FE from almost all carbon structures [6]. The barrier profile is constructed by the method of mirror images using a single image and the field $E_x = -U_a x/d$ overlay [2, 3]. The FN formula stops working exactly at small d, as well as at very large fields. Small d leads to a decrease in the height of the barrier, just as a strong field narrows and sharpens barrier. At the critical field $E_{xc} = 4\pi\varepsilon_0 W^2/e^3$ it disappears [2, 7]. The barrier in this case is described by the function $V(x) = -eE_x x - e^2/(16\pi\varepsilon_0(x+\delta))$ (Fig., curves *2*, *5*). Here $\delta = 0.1$ nm corresponds to $W = 3.6$ eV. For the diode structure the maximum is located in the center $V(d/2) \approx 0$ (Fig., curve *1*). In the presence of field it is reached at a point $x_0 = \sqrt{e/(16\pi\varepsilon_0 E_x)}$. At large fields, it is located almost at the cathode and is equal to $V(x_0) = -2e\sqrt{eE_x/(16\pi\varepsilon_0)}$ (Fig.). The function W depends on the applied field and can vanish at the critical field $E_{xc} = 4\pi\varepsilon_0 W^2/e^3$. Taking $W = 4$ eV, we find a characteristic critical field $E_{xc} = 1.8\cdot 10^{10}$ V/m. It can be obtained by determining the pivot points $x_{1,2}$ from the quadratic equation $eE_x x^2 + xW + e^2/(16\pi\varepsilon_0) = 0$. The disappearance of the barrier at V_F corresponds to the coincidence of the turning points, and the quasi-classical approximation gives the transparency $\mathrm{D}^+(\mathrm{E}) = \mathrm{D}_0(\mathrm{E})\exp\left(-4\sqrt{\mu}W_0^{3/2}/(3\hbar eE_{xc})\right)$ [8]. Here, $\mu = 2m_e$ is the doubled mass of the electron, and W in the sense of this formula is the height of the barrier above the level of kinetic energy, i.e. $W = W_0 = \mathrm{E}_F - \mathrm{E}$. The pre-exponential multiplier is defined in Ref. [8]. Note that the result [8] is obtained for "wide barriers", which does not take place for a triangular barrier, at least in its upper part. The crosslinking of the quasi-classical wave function (WF) with the probability wave at the anode $\psi_a = A_a\exp(ik(x-d))$ should be carried out at the point d on the anode. The tunneling problem is solved strictly and very simply by the exact solution of the Schrödinger equation (SE), for example, by the method of transmission or transfer matrices [9], or by the transformation of wave impedances [10]. The WF and its derivative must be continuous. For a stepwise approximation of the potential $V(x)$, the normalized wave impedance can be defined as $\rho = ik\psi(x)/\psi'(x)$. The numerical solution, even in the absence of a barrier, gives the result 2–3 orders of magnitude smaller than $J^+_{\max}$ [9, 10]. It corresponds to super-strong fields. Let us put $D^+ = 1$ and estimate the current density for $\mathrm{D}^+(\mathrm{E}) = \exp\left(-4\sqrt{\mu}W_0^{3/2}/(3\hbar eE_{xc})\right)$: $J^+ \approx \approx -e\mu\mathrm{E}_F^2 y_0^{1/6}/\left((9\pi^2\hbar^3\right)$, $y_0 = 4\sqrt{\mu}\mathrm{E}_F^{3/2}/(3\hbar eE_{xc})$, which shows the inadequacy of the quasi-classical model in this case. Everywhere above, the + sign indicates tunneling from the cathode to the anode (electron charge $q_e = -e$). The reverse current is possible, due to the reverse tunneling coefficient D^-. Usually $D^- \ll D^+$, its accounting is also significant at low voltages at the anode. For the symmetrical potential $D^+ = D^-$ and the total current is zero: $J = J^+ - J^- = 0$. If we will neglect the reverse current, then $D = D^+$. The general case of thermal field emission current densities has been determined in Ref. [11] as $dJ^{\pm}(U_a,T) = eD^{\pm}(E,U_a)dn^{\pm}_{v_x}$, $dn^{\pm}_{v_x} = j_0 k_B T\ln\left(1+\exp\left(\left(E_{F_c} - E + \mu^{\pm}\right)\left(k_B T\right)\right)\right)dE$. Here k_B is the Boltzmann constant, $\mu^+ = \mu_c = 0$, $\mu^- = \mu_a = -eU_a$ are the chemical potentials. The quantum potential V is determined by the method of multiple images, taking into account small distances $\delta_{c,a} = e^2/(16\pi\varepsilon_0 W_{c,a})$ at the electrodes associated with the function W, which makes it finite [9–13]. There are infinitely many such images (relative to the anode and cathode surfaces), which makes it possible to obtain an accurate profile $V(x)$, including cases of multiple electrodes [9–14], that requires solution of the SE.

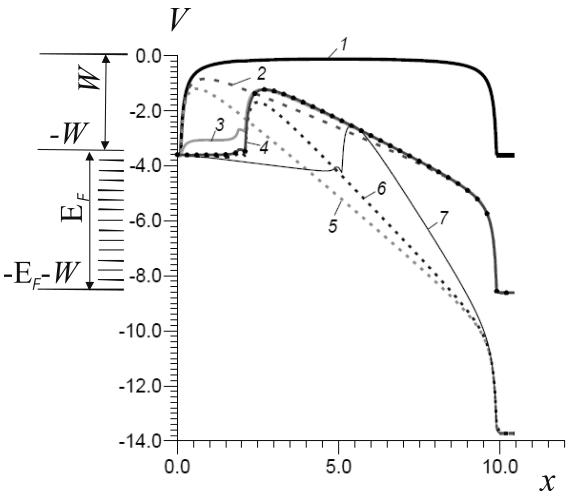

Fig. Distribution of V (eV) in a vacuum diode [16] with a size $d = 10$ nm without a dielectric film (curves *1*, *2*, *5*) and with the film on the cathode of thickness $t = 2$ nm (curves *3*, *4*, *6*) and $t = 5$ nm (curve *7*) depending on distances x (nm) at different anode voltages (V 4): $U_a = 0$ (curve *1*); $U_a = 5$ (curves *2*, *3*, *4*); $U_a = 10$ (curve *5*, *6*, *7*). DP is taken as $\varepsilon = 4$ (curve *3*); $\varepsilon = 10$ (curve *7*); $\varepsilon = 12$ (curves *4*, *6*), $\delta = \delta_d = 0.1$ nm

The next step in refining the model can be based on taking into account the inhomogeneous relief surface [12]. Usually this approach is based on the introduction of a field gain and the use of FN formula. In this case, the local area of the surface is considered as flat. This approximation is usually the basis for the analysis of pointed matrix emission structures such as Spindt cathodes. The creation and research of Spindt cathodes took a long period of time, about 30 years.

Although it is possible to achieve high current densities on very small surfaces of the needles, it was not possible to obtain satisfactory emission sources on such cathodes. They correspond to strong increase in resistance in the area of the tips leading to their heating and explosive emission, poor reproducibility, complex manufacturing technology, a small ratio of the emitting area to the total surface and, accordingly, a small integral current, a strong spread of electrons in velocities, a large operating voltage, poor resistance to reverse ion bombardment and poor durability. Currently, spatially developed nanostructured emitting surfaces mainly made of carbon materials are more promising [6, 15–22]. In such emitters, tunneling is not strictly one-dimensional and follows different trajectories, there are field penetration into the structure [6, 13, 19, 20], porosity and heterogeneity of structures. The emitting surface often significantly exceeds the geometric surface of the cathode [13, 23]. The corresponding models require taking into account the three-dimensional nature of the emitter, solving the Poisson equation (PE), including for determining $V(x)$ taking into account the spatial charge, taking into account field penetration, taking into account nonstationarity, and a number of other approaches. The carbon nanotubes (CNT) emitters [23–25], including in devices [26] and in glass carbon emitters [27–29], are promising. The emitters made of films with carbon nanoclusters [30–35], CNTs nanoclusters [36] and graphene nanoclusters [22, 37] are also used. In a number of works (for example, [34, 35]), the blade and tip structures of FE are analyzed, including structures made of graphene, CNT, glass carbon, graphene, nanoclusters. A comparison of some types of emitters is given in Ref. [37]. The FN formula obtained for emission from metals with flat surfaces stimulated the search for similar formulas for field emission from other structures, including non-planar boundaries, structures with points, semiconductor emitters, cathodes with dielectric films, porous cathodes, carbon structures. The emission mechanisms in them differ significantly. The effect of field penetration, porosity, and the presence of Tamm levels have a significant impact [13]. The penetration of the field significantly depends on the dielectric permittivity (DP), conductivity determined by the concentration of free charges. Therefore, tunneling from structures with semiconductors has special features [38–41]. In the case of solid-state electron plasma, an external electric field leads to the formation of a near-surface charged layer that compensates for the penetration of the field. The thickness of this layer can be estimated taking into account the length of the Debye shielding $L_D = \sqrt{\varepsilon\varepsilon_0 k_B T/N}/e$.

For copper $N = 8.45 \cdot 10^{28}$ m^{-3}, $\varepsilon = 13.1$, we have $L_D = 1.5 \cdot 10^{-11}$ m, i.e. shielding occurs already on one atomic layer. In the case of semiconductors $N \sim 10^{20} - 10^{24}$ m^{-3}, shielding occurs at lengths from 1 to 100 nm, i.e. from 10 to 1000 atomic layers. A low concentration of free charges with the formation of a thin dipole layer of the order of 1 nm leads to a decrease of W. A lower concentration leads to the penetration of the field. The concentration $N > > 10^{25}$ m^{-3} leads to the metallic emission.

In a number of works, attempts have been made to obtain generalizations of the FN formula [42–46], including for non-planar metal emitters. The electrophysical and emission properties of carbon structures, including diamonds, are considered in a number of works, [47–50], as well as tunneling models are analyzed in Refs. [6, 13, 20]. The reasons for low-threshold FE from carbon structures were analyzed. Rigorous quantum theory is based on the density functional theory. The problems of quantum transport and non-stationary tunneling in solid-state structures were considered by solving the SE [51–57] and by self-consistent models with the solution of PE [51, 52] and non-stationary models [55–57]. Equilibrium and nonequilibrium processes in quantum dots, wells and wires, including tunneling, are also considered, including quantum cascade lasers. The literature on RT is mainly devoted to RT diodes. Although these devices achieve a very high current density due to low effective masses, low barrier heights of less than 0.5 eV and their small thicknesses, they cannot be used by vacuum emission electronics. From the point of view of obtaining the maximum current densities, cathode materials with large E_F and a small W are most appropriate. Among them are beryllium with $W = 3.92$ eV, barium with $W = 2.52$ eV and E_F 3.64, as well as with high E_F metals such as Be, Ni, Al, Ag, Cu. It is not advisable to use strong fields in terms of obtaining long-lasting cathodes. For high-current sources, the emission surface should be large, and the V shape should be multi-welled. Many publications are devoted to point sources and their arrays [58–62]. The use of Spindt-type matrices did not lead to breakthrough successes due to explosive emission [59].

1. Tunneling and field emission in multi-barrier 1D structures

Let the barrier be described by a potential function V with the Fermi level (FL) $V(0) = V_F = -W$ at the cathode. The value $V(d) = -W - eU_a$ is

the FL at the anode. The profile V has all negative values if a free electron in vacuum corresponds to zero potential energy. This value $V(d/2) \approx 0$ is achieved at very large d. Using the method of multiple images, the function $W(x, \delta_c, \delta_a, d)$ has been obtained in Refs. [9–13]. This function takes into account an infinite series of images relative to the cathode and anode and determines the potential energy of an electron at point x as the work of moving it from the cathode. At the cathode the work function is $W(0, \delta, \delta_a, d) = -e^2 (16\pi\varepsilon_0)^{-1} \{\delta^{-1} - 2d^{-1}\}$. Here $W(0, \delta_{\tilde{n}}, \delta_a, d) = -e^2 (16\pi\varepsilon_0\delta)^{-1} = -W_a$, $d \gg \delta \gg \delta_{c,a}$. In the case $W_c = W_a$ we put $\delta_{c,a} = \delta$. The characteristic size $\delta = 0.1$ nm corresponds to $W = 3.6$ eV. The electron density $d\rho(x) = |\psi(x, \mathrm{E})|^2$ can be found if the WF $\psi(x, \mathrm{E})$ is defined from the SE taking into account the electron energy distribution. Here the incident WF is $\psi^+(x, \mathrm{E}) = a^+(\mathrm{E}) [\exp(ikx) + R(\mathrm{E}) \exp(-ikx)]$, $a^+(\mathrm{E}) = m_e (E_{Fc} - E(k)) / (2\pi^2\hbar^3)$ is the density of electrons with the energy E running to the barrier [2], where R is reflection. If the density J^+ is small, it is possible to solve the problem iteratively by choosing a barrier profile without taking into account $\rho(x)$ and the solution of the PE. For 3D tunneling of a single electron along the trajectory $y = y_0(x)$, $z = z_0(x)$, it is necessary to sum up the density of transparency along all trajectories [12]. These trajectories need to be determined and barrier profiles calculated along them. Approximately, we can assume that electrons move along lines of force, but in general it is necessary to solve the equations of motion. In the case of an uneven cathode surface $x = X(y, z)$, it is possible to approximate the images at symmetrical points $-x'$ relative to this surface and reduce the 3D SE to one-dimensional ones. This approach allows one to replace the 3D tunneling by a series of 1D ones and the current can be calculated as the sum of tunnel currents along various trajectories [12]. The FN formula is often used for this purpose for surface areas, which is a more rough approximation.

The uneven surface allows one to increase the local emission, though not so much as to talk about approaching the limit current. At the voltage at the anode U_a, the quantum potential is defined as $V(x) = W(x, \delta_c, \delta_a, d) - eU_a x/d$. The maximum of the function (4) is located in the center $W(d/2) = -e^2 \ln 2 / (4\pi\varepsilon_0 d)$ for $U_a = 0$. The anode voltage strongly shifts it to the cathode. The smaller the d and greater U_a and E, the more the FN formula is violated. If there are grids located at the same potentials, the image method in the form (4) can be used for all vacuum gaps. At the same time, the WF should be introduced for grids. The calculation of barrier profiles with three and four electrodes is given in Ref. [10]. For all such structures, there are RT when $R = 0$, and there is complete transparency $D^+ = 1$. The simplest result is obtained for rectangular potential models. The energy levels in RT structures $\mathrm{E}_n = \mathrm{E}'_n - i\mathrm{E}''_n$ are metastable, and when $\mathrm{E} = \mathrm{E}'_n$, the RT occurs. E''_n defines the width of the level. Such levels are possible if $V/2 < \mathrm{E}_n < V$. For wide barriers, electronic waves do not leak through them, i.e. the metastable levels turn into eigenlevels. For the lower level $\mathrm{E}_1 \approx V/2$ we have $\mathrm{E}_1 = \pi^2\hbar^2 / (4\mu t_g^2)$. For the upper level $\mathrm{E}_n \approx V$, since the tangent argument is small, $\mathrm{E}_n \approx 2\hbar^2 \left(\sqrt{1 + t_g^2 V \mu / \hbar^2} - 1 \right) / (\mu t_g^2)$. The barrier profiles shown in Ref. [63] demonstrate the peaks of the transmission coefficient. In an asymmetric structure with a voltage at the anode, two or more grids are needed for RT [9]. The total current density $J = J^+ - J^-$ is determined mainly by the forward current, since the reverse current at the anode voltages taken is negligible. Heterostructures with multiple grids lead to the appearance of transmission zones. Let the specified zone $\Delta\mathrm{E}$ be in the range $0 < \mathrm{E}_1 < \mathrm{E} < \mathrm{E}_2 < \mathrm{E}_F$. In this case we have $J^+ = em_e\pi^{-2}\hbar^{-3}\mathrm{E}_F\Delta\mathrm{E}\left(1 - \left(\mathrm{E}_1 + \mathrm{E}_2\right)/\left(2\mathrm{E}_F\right)\right)/2$. If $\Delta\mathrm{E}$ is located in the center of the conduction band and $\Delta\mathrm{E} = 0.01\mathrm{E}_F$, then we get $J^+ = 0.5 \cdot 10^{-2} J^+_{\max}$, i.e. we can approach the limiting density. Tunneling without loss of momentum is possible at a length significantly shorter than the free path length. For metals at $T = 300$ K, this length is of the order of 30–50 nm, i.e. the thickness of the structure should not exceed 10 nm. Excluding vacuum gaps and counting the grid size of the order of 1 nm, we obtain the number of possible grids of no more than 5. The creation of grids is possible using carbon CVD technologies [47–50], using graphene and CNT. Graphene grid structures and CNT grids are promising, for example, in the form of a woodpile. It is enough to use fields of no more than 10^{10} V/m. For vacuum electronics, it is advisable to perform low-voltage sources with an anode in the form of a grid, and the electrons flying through it are accelerated to the desired energies by a second anode. For numerical solution of the SE, it is convenient to use a step representation of V. The potential is constant in the wells, and each grid electrode is described by a single step function. Each function corresponds to a transmission matrix with well-known matrix elements [9]. The SE solution program consists in constructing a complete matrix $\hat{T} = \hat{T}_1\hat{T}_2 \ldots \hat{T}_N$ by multiplying the matrices of the regions and calculating the transmission coefficient from the system

of equations $1+R=(T_{11}-iT_{12}/k)T$, $1-R=$ $=ik_0(T_{21}-iT_{22}/k)T$ [9–12]. We have the following result $T=2/[T_{11}+T_{22}(k_0/k)+i(k_0T_{21}-T_{12}/k)]$, $R=1-k_0\big(T_{21}-iT_{22}/k\big)T$. Since also $Z=$ $=(1+R)/(1-R)=(kT_{11}-iT_{12})/(ik_0kT_{21}+k_0T_{22})$, then $R=(Z-1)/(Z+1)$. The calculated transparency (tunneling) coefficient of the barrier $D^+(\mathrm{E})=1-|R|^2$ depends on the kinetic energy of the electron at the cathode. The notations used here are $k_0=\sqrt{\mu\mathrm{E}}/\hbar$, $k=\sqrt{\mu(\mathrm{E}+eU_a)}/\hbar$. To solve the SE 152 steps in the approximation were used in the calculations [9]. For the synthesis of RT structures, it is necessary to determine metastable levels E_n. The task is posed as a crosslinking of the WF structure with the WF $\psi_1(x)=a_1\exp(-ik_{0n}x)$ at the cathode and the WF $\psi_2(x)=a_2\exp(ik_n(x-d))$ at the anode, where $k_{0n}=\sqrt{\mu_e(\mathrm{E}_n-V_g)}/\hbar$, $k_n=$ $=\sqrt{\mu_e(\mathrm{E}_n-V_g+V_a)}/\hbar$. In the case of a well, proper levels $E_n<V_g-V_a$ are possible, and then both wave numbers are imaginary, and evanescent outside the structure of the WF. Solving the problem by the method of transmission matrices taking into account the ratio $k_n^2=k_{0n}^2+\mu_eV_a/\hbar^2$, we find $k_{0n}=$ $=i\big(T_{21}+ik_nT_{22}\big)/\big(T_{11}+ik_nT_{12}\big)$. This nonlinear transcendental equation defines the roots E_n. The synthesis task is to obtain a potential profile V that ensures the location of metastable levels in the widest possible band as close as possible to the cathode conduction band. The convenient method for solving the SE consists in the transformation of the wave impedance [63–68].

2. Effects of thermal field emission, field penetration, spatial charge

Thermal field emission has been studied in a number of papers, for example [10, 11, 64–68]. Thermal emission prevails in diode structures at low voltages, and field emission dominates at high voltages [64]. In resonant tunnel structures, a strong increase in current leads to heating of the cathode and anode, which requires solving the thermal problem and thermal field emission [10]. The size of the potential barrier in strong fields that allow significant tunneling is of the order of 1–3 nm. The penetration of the field to depths of this order can significantly change the barrier. The effect was first noted in Refs. [18–20]. The penetration is possible if there is a homogeneous dielectric film with DP ε of a nanoscale thickness t_d on the cathode, or a semiconductor film, or an inhomogeneous structure described by an effective DP. The penetration of the field reduces the barrier for the cathodes with BaO film [2]. If the penetrating field is considered constant, all charges are displaced, forming a double electric dipole layer with a surface charge density on the outer surface. The field of such a flat capacitor weakens the penetrating field and almost eliminates the barrier at the metal-film boundary. Electrons exit the metal into the film, and a barrier appears at the film-vacuum boundary. In general, it is necessary to solve the PE together with the SE, especially for high emission current density [63]. In the area in front of the single barrier $R\approx-1$, the density is usually small and strongly decreases inside the barrier to its rear. At RT $R\approx0$, and the density is determined by the incident flow. The joint solution of the SE and PE is a nonlinear iterative problem [51–54]. The spatial charge in the barrier area leads to its increase, which limits the current. It is possible to correct this effect in multielectrode structures by changing the electrostatic potentials of the electrodes or by changing their W. The problem for the dielectric film was solved in Refs. [12, 13]. The essence of the solution is that infinite series of images are constructed relative to the surface of the film, cathode and anode. The electrostatic Green function of a point charge in a flat capacitor with a film is found. Examples of constructing barriers for a dielectric film with thickness t_d at the cathode are shown in Fig. The inhomogeneous film improves tunneling, therefore, one of the tasks may be the synthesis of the DP profile, contributing to the maximum of J. A double electric layer appears in a thin, well-conducting film. It works as a dipole that reduces the external field. With a large DP, the barrier on the cathode-film section is practically absent and appears only in the region of its boundary with vacuum (Fig.). The penetration of the field into the film region can lead to acceleration and to a negative slope $V(x)$ up to the boundary with vacuum (curve *7*, Fig.). Porous films from diamond-graphite nanoclusters increase the emissions [15–20]. Porosity and the presence of a dielectric phase lead to the penetration of the field, as well as to the presence of surface levels at the boundaries of clusters. A part of the emission goes to these levels, and from them into a vacuum [13]. For carbon structures, the ionization potential and the function W calculated by quantum methods and measured have the order of eV. A diamond-graphite film on a metal cathode works in such a way that the FN formula recalculation for the corresponding homogeneous cathode gives an effective W is 1–2 orders of magnitude less [6, 21, 22]. The work of moving the charge in the film is about one time less than a similar work without the film. Reducing the DP of the film at this boundary decreases the barrier, that can be done by profiling. Diamond-

graphite films demonstrating high low-voltage emission have just such a surface structure consisting of clusters with sizes of several nm. The presence of conducting phases in the film is equivalent to an increase in the effective DP. The film effect is that the field penetrates into the dielectric and accelerates the electron. This is manifested in the slope of the function $V(x)$ to the barrier in vacuum (curve 7, Fig.). The energy of the electron impinging on the barter in a wide film can increase significantly to a value of several eV. In such structures, double-humped functions V and even RT are possible [13]. The penetration of the field is observed in all carbon structures at the cathode [18]. The FE of such structures is considered in many publications (see [6, 13, 15–18]). Carbon exhibits the largest number of allotropic modifications with significantly different properties and a variety of electronic structures, due to a different ratio of sp^1-, sp^2- and sp^3-hybridized atoms. It implements a range of electrical conductivity from a dielectric (diamond) to graphite. There are such modifications as soot, black coal, carbine, fullerenes, single-layer and multilayer CNTs, carbon filaments, graphene nanofibers, various structures of amorphous carbon (glass carbon) and pyrocarbon. All of them are more or less porous and heterogeneous. In porous structures there are surfaces in contact with vacuum channels and Tamm's levels. The emission comes from the entire surface through different channels and trajectories. There are chaotic structures such as glass carbon and quasi-periodic structures such as column graphene [13] or woodpile. In the first case, the effective DP can be used for modeling. In the second case, models with quasi-periodic structures should be considered [12]. Structures with diamond-graphite clusters on the cathode obtained by magnetron sputtering in low-pressure plasma are promising [13]. Comparison with the FN formula shows that in carbon films, the effective work function W decreases to 0.1 eV [6]. The field penetration and surface levels during nonstationary tunneling lead to hysteresis [6, 13]. The field penetration also occurs in semiconductor cathodes [2]. An example is oxide cathodes from BaO, which have a low W of the order of 1 eV or less [2]. Ba ions in such a film form donor levels, and the film itself, when doped, can acquire the properties of an n-type semiconductor.

3. Non-stationary tunneling

Non-stationary tunneling and especially RT has been considered in a number of papers [52–57] in connection with the tasks of modeling resonant tunneling diodes and transistors. Transients in such devices are considered in Refs. [53–55]. High currents at RT can lead to strong heat generation. Since it occurs due to the interaction of electrons with phonons, this also justifies the use of ultra-low temperatures. With vacuum RT, the Nottingham effect may increase, which requires cooling of the cathode. Each electron hitting the anode transfers eU_a energy to it. Due to the complexity, such problems are usually solved in a one-dimensional approximation with a joint solution of non-stationary SE and PE [56,57]. Accordingly, the boundary conditions consist in the crosslinking of the WF and their derivatives in the cathode region, the tunneling region and the anode. One can solve the problem with zero boundary conditions $\Phi(0,t) = \Phi(d,t)$ and then add a linear potential xU_a/d. The SE should be solved by setting the incident particle flow from the cathode and from the anode. The first one does not depend on time, while the second one may be time-dependent when the anode voltage changes. If the anode voltage is high, it can be lowered. In this case, the luminaries R and T depend on time. The solution can be obtained by the time series method, by the method of integral equations using the propagator Green function for the SE [56], by numerical methods [54].

4. High-current emission structures

The current densities of the order 10^{12}–10^{13} A/m^2 were theoretically obtained in structures with RT in Refs. [9, 10, 63]. Vacuum nanoscale structures with single and double grids are considered. Refs. [9, 64] indicate the operating temperature at high current densities [10] and the spatial charge effect [64]. The latter can be compensated by changing the potentials on the electrodes. The heat sink requires a massive thermostat. Heat release at RT occurs due to the Nottingham effect and the contribution from Joule heat. The solution to the heat dissipation problem can be obtained by using cryogenic temperatures. The best materials are CVD carbon films [47–50]. At the same time, layers with sp^3 and sp^2 hybridizations should be alternated to perform multi-layer and multi-barrier structures. The best material for barriers is a crystalline diamond with DP 5.6, which has a unique thermal conductivity. For thin barriers, it is an amorphous CVD diamond with sp^3 hybridization of 80–88% [47] at $\varepsilon = 4.94$–5.6 and the band gap of 4.5 eV. Performing a heterostructure with a double grid with a positive potential U_g of several Volts on it, it is possible to obtain high-precision electron sources. For emission electronics, a large integral beam current is important [4], which it is desirable to perform as a ribbon electron beam. A large integral current can be obtained by having a

large emission surface with a high current density. Beams that are wide in one transverse dimension and thin in the other are important. Such beams are convenient to use in decelerating systems such as "comb", "double shifted comb", "looping waveguide" in TWT millimeter and THz bands. An increase in the beam current can be achieved by increasing the width. As high-current emitters with FE, blade-type structures with multi-row parallel graphene sheets, and a point-type structure in the form of a forest of CNTs are possible. There are sufficiently developed technologies for creating such arrays from CNTs and nanowires. Their advantage is a good penetration of the field with a large gain on atomically sharp edges and a large surface involved in the emission. The field penetrates into such a structure, so the emission also comes from the surface of graphene sheets or from the surface of CNTs. The beam can be made very wide in one direction, and in the other, with a large number of periods, its compression allows one to get a wide and thin ribbon beam. Another approach can be based on emission from spatially developed surfaces formed by carbon structures [6, 16–20]. To increase the current, their emitting surfaces can be positioned tangentially to the plane of the forming ribbon beam and use a 90-degree rotation of the trajectories of normally departing electrons [69].

Conclusions

1. The current densities 2–3 orders of magnitude lower than the limit values 10^{16} A/m^2 are theoretically achievable [9, 10]. The optimal RT structure is a two-well and three-barrier. Structures with RT with a wide energy band and located below FL are optimal. Such a structure can be created as an alternation of CVD diamond and conductive carbon or Be films. The use of grids prevents the reverse ion bombardment of the cathode. The free path length of the electrons should significantly exceed the size of the structures, for which ultra-low temperatures are perspective. At room temperatures, the size of 10 nm is the limit. Multilayer graphene, CNT of metallic type, CVD conductive carbon with predominant sp^2 hybridization, and amorphous CVD sp^3 diamond can serve as convenient materials for grids and dielectric films (barriers). Wide grids are promising for increasing the number of resonant levels.

2. Since the tunneling effect is associated with nanoscale barriers, all objects can be divided into structures of nanoelectronics and microelectronics with operating voltages of the order of Volts and kilovolts, respectively. For their production, well-developed technologies for creating thin-film structures are used: vacuum spraying, magnetron sputtering from low-pressure plasma, CVD technologies, photolithography, MOM, MOS, MIM, MIS and similar technologies. This is followed by the possibility of using a structures type of MOS and MIM with a single-stage level and even more [70], as well as an additional structure with graphene. In the latter case, the anode is made thin (usually made of gold) and transparent for the flight of electrons into a vacuum and further use of the beam [70]. There are two possibilities here, namely, to use multilayer graphene for quantum wells or to create multi-barrier structures with several narrow wells. A difficult technological task that has not been fully solved is the cultivation of epitaxial graphene on substrates, the creation of hanging graphene grids and the creation of structures with several electrodes. Structures with a wide pit or with several pits seem to be more effective.

Various mechanisms of the FE formation have been examined in the review. For some structures without RT, a significant increase in the current density is possible. Carbon structures and carbon coatings are promising for this. Emission structures allowing to obtain high current ribbon electron beams have been considered. An increase in the current density and the integral beam current can be achieved due to the spatial addition of several emitters and due to the rotation of the trajectories of electrons flying from large surfaces, as well as due to compression.

3. Non-stationary tunneling, nonlinear response of structures, joint solution of the SE, PE and Fourier equations (thermal conductivity), creation of structures with standing high current densities can be noted as unsolved research problems.

References

1. Fowler R. H., Nordheim L. Electron Emission in Intense Electric Fields. *Proc. Royal Soc. A*, 1928, vol. 119, iss. 781, pp. 173–181. https://doi.org/10.1098/RSPA.1928.0091
2. Proskurovskij D. I. *Emissionnaya electronika* [Emission electronics]. Tomsk, TSU Publ., 2010. 280 p. (in Russian).
3. Fursey G. N. *Field emission in vacuum micro-electronics*. New York, Kluwer Academic Plenum Publishers, Springer, 2005. 205 p.
4. Burtsev A. A., Grigor'ev Yu. A., Danilushkin A. V., Shumikhin K. V. Features of the Development of Electron-Optical Systems for Pulsed Terahertz Traveling-Wave Tubes (Review). *Tech. Phys.*, 2018, vol. 63, no. 3, pp. 452–459. https://doi.org/10.1134/S1063784218030040
5. Egorov N., Sheshin E. *Field Emission Electronics*. Springer Series in Advanced Microelectronics. New York, Springer, 2017. Vol. 60. 568 p.

6. Eidelman E. D., Arkhipov A. V. Field emission from carbon nanostructures: Models and experiment. *Phys. Usp.*, 2020, vol. 63, no. 7, pp. 648–667. https://doi.org/10.3367/UFNe.2019.06.038576
7. Bushuev N. A. Tunnel current and I–V characteristics of vacuum extremely-high-frequency microelectronic structures. *J. Commun. Technol. Electron.*, 2015, vol. 60, iss. 2, pp. 193–200. https://doi.org/10.1134/S1064226915020023
8. Davydov A. S. *Quantum Mechanics*. New York, Pergamon Press, 1965. 637 p.
9. Davidovich M. V., Nefedov I. S., Glukhova O. E., Slepchenkov M. M. Toward the theory of resonant-tunneling triode and tetrode with CNT-graphene grids. *J. Appl. Phys.*, 2021, vol. 130, iss. 20, art. 204301. https://doi.org/10.1063/5.0067763
10. Davidovich M. V., Nefedov I. S., Glukhova O. E., Rubi J. M. Field emission in vacuum resonant tunneling heterostructures with high current densities. *Sci. Rep.*, 2023, vol. 13, iss. 1, art. 19365. https://doi.org/10.1038/s41598-023-44900-2
11. Davidovich M. V. Thermal-field emission in nanostructures with resonant tunneling. *Tech. Phys.*, 2024, vol. 69, no. 1, pp. 29–43. https://doi.org/10.61011/JTF.2024.01.56899.170-23
12. Davidovich M. V., Yafarov R. K. Field-Emission Staggered Structure Based on Diamond–Graphite Clusters. *Tech. Phys.*, 2018, vol. 63, no. 2, pp. 274–284. https://doi.org/10.1134/S106378421802010X
13. Davidovich M. V., Yafarov R. K. Pulsed and Static Field Emission VAC of Carbon Nanocluster Structures: Experiment and Its Interpretation. *Tech. Phys.*, 2019, vol. 64, no. 8, pp. 1210–1220. https://doi.org/10.1134/S106378421908005X
14. Simmons J. G. Generalized formula for the electric tunnel effect between similar electrodes separated by a thin insulating film. *J. Appl. Phys.*, 1963, vol. 34, iss. 6, pp. 1793–1803. https://doi.org/10.1063/1.1702682
15. Obraztsov A. N., Pavlovsky I. Yu., Volkov A. P. Field electron emission in graphite-like films. *Tech. Phys.*, 2001, vol. 46, no. 11, pp. 1437–1443. https://doi.org/10.1134/1.1418509
16. Bobkov A. F., Davydov E. V., Zaitsev S. V., Karpov A. V., Kozodaev M. A., Nikolaeva I. N., Popov M. O., Skorokhodov E. N., Suvorov A. L., Cheblukov Yu. N. Some aspects of the use of carbon materials in field electronic emission cathodes. *J. Vac. Sci. Technol. B*, 2001, vol. 19, iss. 1, pp. 32–38. https://doi.org/10.1116/1.1340017
17. Fursey G. N., Petrik V. I., Novikov D. V. Low-threshold field emission from carbon nanoclusters obtained by the method of cold destruction of graphite. *Tech. Phys.*, 2009, vol. 54, no. 7, pp. 1048–1052. https://doi.org/10.1134/S1063784209070202
18. Forbes R. G. Low-macroscopic-field electron emission from carbon films and other electrically nanostructured heterogeneous materials: Hypotheses about emission mechanism. *Solid-State Electronics*, 2001, vol. 45, no. 6, pp. 779–808. https://doi.org/10.1016/S0038-1101(00)00208-2
19. Forbes R. G. Exact analysis of surface field reduction due to field-emitted vacuum space charge, in parallel-plane geometry, using simple dimensionless equations. *J. Appl. Phys.*, 2008, vol. 104, iss. 8, art. 084303. https://doi.org/10.1063/1.2996005et
20. Forbes R. G., Xanthakis J. P. Field penetration into amorphous-carbon films: Consequences for field-induced electron emission. *Surf. Interface Anal.*, 2007, vol. 39, iss. 2–3, pp. 139–145. https://doi.org/10.1002/sia.2477
21. Voznyakovsky A. P., Fursey G. N., Voznyakovsky A. A., Polyakov M. A., Neverovskaya A. Yu., Zakirov I. I. Low-threshold field electron emission from two-dimensional carbon structures. *Tech. Phys. Lett.*, 2019, vol. 45, no. 5, pp. 467–470. https://doi.org/10.21883/PJTF.2019.09.47715.17705
22. Fursey G. N., Polyakov M. A., Cantonistov A. A., Yafyasov A. M., Pavlov B. S., Bozhevolnov V. B. Field and explosive emissions from graphene-like structures. *Tech. Phys.*, 2013, vol. 83, no. 6, pp. 845–851. https://doi.org/10.1134/S1063784213060121
23. Eletskii A. V. Carbon nanotube-based electron field emitters. *Phys. Usp.*, 2010, vol. 53, no. 3, pp. 863–892. https://doi.org/10.3367/UFNe.0180.201009a.0897
24. De Jonge N., Bonard J.-M. Carbon nanotube electron sources and applications. *Philosophical Trans. Royal Soc. A*, 2004, vol. 362, iss. 1823, pp. 2239–2266. https://doi.org/10.1098/rsta.2004.1438
25. Hojati-Talemi P., Hawkins S., Huynh C., Simon G. P. Understanding parameters affecting field emission properties of directly spinnable carbon nanotube webs. *Carbon*, 2013, vol. 57, pp. 388–394. https://doi.org/10.1016/j.carbon.2013.01.088
26. Zeng B., Ren Z. Field Emission of Carbon Nanotubes. In: Shi D., ed. *Nano Science in Biomedicine*. Berlin, Heidelberg, Springer, 2009, pp. 586–617. https://doi.org/10.1007/978-3-540-49661-8_23
27. Léonard F. *The Physics of Carbon Nanotube Devices*. New York, William Andrew Inc., 2009. 310 p.
28. Arkhipov A., Davydov S., Gabdullin P., Gnuchev N., Kravchik A., Krel S. Field-Induced electron emission from nanoporous carbons. *J. Nanomaterials*, 2014, vol. 20014, art. 190232. https://doi.org/10.1155/2014/190232
29. Arkhipov A. V., Gabdullin P. G., Mishin M. V. On possible structure of field-induced electron emission centers of nanoporous carbon. *Fuller. Nanotub. Carbon Nanostruct.*, 2010, no. 1–2, pp. 86–91. https://doi.org/10.1080/1536383X.2010.490149
30. Glukhova O. E., Slepchenkov M. M. Electronic properties of the functionalized porous glass-like carbon. *J. Phys. Chem. C*, 2016, vol. 120, iss. 31, pp. 17753–17758. https://doi.org/10.1021/acs.jpcc.6b05058
31. Arkhipov A. V., Mishin M. V. Interpretation of dynamic and dc field-emission characteristics of nanocarbons in terms of two-stage emission model. *Fuller. Nanotub. Carbon Nanostruct.*, 2010, no. 1–2, pp. 75–80. https://doi.org/10.1080/1536383X.2010.490146
32. Arkhipov A. V., Eidelman E. D., Zhurkin A. M., Osipov V. S., Gabdullin P. G. Low-field electron emission from carbon cluster films: Combined thermoelectric/hot-

electron model of the phenomenon. *Fuller. Nanotub. Carbon Nanostruct.*, 2020, vol. 28, no. 4, pp. 286–294. https://doi.org/10.1080/1536383X.2019.1708727

33. Arkhipov A. V., Gabdullin P. G., Gnuchev N. M., Emel'yanov A. Yu., Krel' S. I. Low-voltage field emission from carbon films produced by magnetron sputtering. *Tech. Phys. Lett.*, 2014, vol. 40, no. 12, pp. 1065–1068. https://doi.org/10.1134/S1063785014120037
34. Dzbanovsky N. N., Minakov P. V., Pilyavsky A. A., Rakhimov A. T., Seleznev B. V., Suetin N. V., Yuryev A. Yu. High-current electron gun with a field-emission cathode and diamond grid. *Tech. Phys.*, 2005, vol. 50, no. 10, pp. 1360–1362. https://doi.org/10.1134/1.2103286
35. Aban'shin N. P., Avetisyan Yu. A., Akchurin G. G., Loginov A. P., Morev S. P., Mosiyash D. S., Yakunin A. N. A planar diamond-like carbon nanostructure for a low-voltage field emission cathode with a developed surface. *Tech. Phys. Lett.*, 2016, vol. 42, no. 5, pp. 509–512. https://doi.org/10.1134/S1063785016050175
36. Aban'shin N. P., Gorfinkel' B. I., Morev S. P., Mosiyash D. S., Yakunin A. N. Field emission structures of nanosized carbon with ionic protection structures. *Tech. Phys. Lett.*, 2014, vol. 40, no. 5, pp. 404–407. https://doi.org/10.1134/S1063785014050022
37. Konakova R. V., Okhrimenko O. B., Svetlichnyi A. M., Ageev O. A., Volkov E. Yu., Kolomiytsev A. S., Jityaev I. L., Spiridonov O. B. Characterization of Field Emission Cathodes Based on Graphene Films on SiC. *Semiconductors*, 2015, vol. 49, no. 9, pp. 1242–1245. https://doi.org/10.1134/S1063782615090146
38. Shesterkin V. I. Emission and operational characteristics of various type of field emission cathodes. *J. Comm. Tech. Electron.*, 2020, vol. 65, no. 1, pp. 1–26. https://doi.org/10.31857/S0033849420010040
39. Stratton R. Theory of Field Emission from Semiconductors. *Phys. Rev.*, 1962, vol. 125, iss. 1, pp. 67–82. https://doi.org/10.1103/PhysRev.125.67
40. Murzin V. N., Mityagin Yu. A. Resonance tunneling, electric and optical phenomena in long-period semiconductor superlattices. *Phys. Usp.*, 1999, vol. 42, no. 4, pp. 396–399. https://doi.org/10.1070/PU1999v042n04ABEH000459
41. Arseev P. I., Mantsevich V. N., Maslova N. S., Panov V. I. Tunneling features in semiconductor nanostructures. *Phys. Usp.*, 2017, vol. 60, no. 11, pp. 1067–1086. https://doi.org/10.3367/UFNe.2017.01.038055
42. He J., Cutler P. H. Generalization of Fowler–Nordheim field emission theory for nonplanar metal emitters. *Appl. Phys. Lett.*, 1991, vol. 59, iss. 13, pp. 1644–1648. https://doi.org/10.1063/1.106257
43. Fursey G. N., Glazanov D. V. Deviations from the Fowler–Nordheim theory and peculiarities of field electron emission from small-scale objects. *J. Vac. Sci. Technol. B*, 1998, vol. 16, iss. 2, pp. 910–915. https://doi.org/10.1116/1.589929
44. Forbes R. G., Deane J. H. B. Reformulation of the standard theory of Fowler–Nordheim tunnelling and cold field electron emission. *Proc. Royal Soc. A*, 2007, vol. 463, iss. 2087, pp. 2907–2927. https://doi.org/10.1098/rspa.2007.0030
45. Forbes R. G. Physics of generalized Fowler–Nordheim-type equations. *J. Vac. Sci. Technol. B*, 2008, vol. 26, iss. 2, pp. 788–793. https://doi.org/10.1116/1.2827505. S2CID 20219379
46. Kyritsakis A., Xanthakis J. P. Derivation of a generalized Fowler–Nordheim equation for nanoscopic field-emitters. *Proc. Royal Soc. A*, 2015, vol. 471, iss. 2174, art. 20140811. https://doi.org/10.1098/rspa.2014.0811
47. Robertson J. Diamond-like amorphous carbon. *Materials Science and Engineering R: Reports*, 2002, vol. 37, iss. 4–6, pp. 129–281. https://doi.org/10.1016/S0927-796X(02)00005-0
48. Sunil D., Vankar V. D., Chopra K. L. Infrared and ellipsometric studies of amorphous hydrogenated carbon films. *J. Appl. Phys.*, 1991, vol. 69, iss. 6, pp. 3719–3722. https://doi.org/10.1063/1.348464
49. Dmitriev V. K., Il'ichev E. A., Kirpilenko G. G., Petrukhin G. N., Rychkov G. S., Frolov V. D. Characteristics of amorphous silicon-carbon and metal-silicon-carbon films, areas of possible applications. Review. *Proc. Universities. Electronics*, 2023, vol. 28, no.1, pp. 24–48 (in Russian). https://doi.org/10.24151/1561-5405-2023-28-1-24-48
50. Giubileo F., Di Bartolomeo A., Lemmo L., Luongo G., Urban F. Field Emission from Carbon Nanostructures. *Appl. Sci.*, 2018, vol. 8, iss. 4, art. 526. https://doi.org/10.3390/app8040526
51. Sun J. P., Haddad G. I., Mazumder P., Schulman J. N. Resonant tunneling diodes: Models and properties. *Proc. IEEE*, 1998, vol. 86, no. 4, pp. 641–660. https://doi.org/10.1109/5.663541
52. Elesin V. F. Theory of coherent generation in resonant-tunneling diodes. *JETP*, 1999, vol. 89, no. 8, pp. 377–383. https://doi.org/10.1134/1.558994
53. Kluksdahl N. C., Kriman A. M., Ferry D. K. Self-consistent study of the resonant-tunneling diode. *Phys. Rev. B*, 1989, vol. 39, iss. 11, art. 7720. https://doi.org/10.1103/PhysRevB.39.7720
54. Pinaud O. Transient simulations of a resonant tunneling diode. *J. Appl. Phys.*, 2002, vol. 92, iss. 4, pp. 1987–1994. https://doi.org/10.1063/1.1494127
55. Mennemann J. F., Jungel A., Kosina H. Transient Schrodinger-Poisson Simulations of a High-Frequency Resonant Tunneling Diode Oscillator. *J. Comput. Phys.*, 2013, vol. 239, pp. 187–205. https://doi.org/10.1016/j.jcp.2012.12.009
56. Grishakov K. S., Elesin V. F. Transition times between the extremum points of the current–voltage characteristic of a resonant tunneling diode with hysteresis. *Semiconductors*, 2016, vol. 50, no. 8, pp. 1092–1096. https://doi.org/10.1134/S1063782616080121
57. Davidovich M. V. Time-dependent resonant tunneling in a double-barrier diode structure. *JETP Lett.*, 2019, vol. 110, no. 7, pp. 472–480. https://doi.org/10.1134/S0370274X19190068
58. Spindt C. A. Physical properties of thin-film field emission cathodes with molybdenum cones. *J. Appl. Phys.*,

1976, vol. 47, iss. 12, pp. 5248–5263. https://doi.org/10.1063/1.322600

59. Dyke W. P., Trolan J. K. Field emission: Large current densities, space charge, and the vacuum arc. *Phys. Rev.*, 1953, vol. 89, iss. 4, pp. 799–808. https://doi.org/10.1103/PhysRev.89.799
60. Everhart T. E. Simplified analysis of point-cathode electron sources. *J. Appl. Phys.*, 1967, vol. 38, iss. 13, pp. 4944–4957. https://doi.org/10.1063/1.1709260
61. Smith R. C., Forrest R. D., Carey J. D., Hsu W. K., Silva S. R. P. Interpretation of enhancement factor in non-planar field emitters. *Appl. Phys. Lett.*, 2005, vol. 87, iss. 1, art. 013111. https://doi.org/10.1063/1.1989443
62. Forbes R. G. Description of field emission current/voltage characteristics in terms of scaled barrier field values (f-values). *J. Vacuum Sci. Technol. B*, 2008, vol. 26, iss. 1, pp. 209–2013. https://doi.org/10.1116/1.2834563
63. Cabrera H., Zanin D. A., De Pietro L. G., Michaels Th., Thalmann P., Ramsperger U., Vindigni A., Pescia D. Scale invariance of a diodelike tunnel junction. *Phys. Rev. B*, 2013, vol. 87, iss. 11, art. 115436. https://doi.org/10.1103/PhysRevB.87.115436
64. Davidovich M. V. Peculiarities of Vacuum Resonant Tunneling at One- and Two-Well Barrier Potentials. *Tech. Phys.*, 2022, vol. 67, no. 9, pp. 361–375. https://doi.org/10.1134/S1063784222060019
65. Jensen K. L. General thermal-field emission equation. *Appl. Phys. Lett.*, 2006, vol. 88, art. 154105. https://doi.org/10.1063/1.2193776
66. Liang S.-D. Theory of field emission. *Europ. Phys. J. B*, 2018, vol. 91, art. 182. https://doi.org/10.1140/epjb/e2018-90181-x
67. Herring C., Nichols M. Thermionic Emission. *Rev. Mod. Phys.*, 1949, vol. 21, no. 2, pp. 185–270. https://doi.org/10.1103/RevModPhys.21.185
68. Murphy E. L., Good R. H. Thermionic Emission, Field Emission, and the Transition Region. *Phys. Rev.*, 1956, vol. 102, iss. 6, pp. 1464–1473. https://doi.org/10.1103/PhysRev.102.1464
69. Davidovich M. V. High-current field emission nanostructure with a ribbon beam. *Tech. Phys. Lett.*, 2024, vol. 50, no. 8, pp. 22–25. https://doi.org/10.61011/PJTF.2024.16.58533.19626
70. Fitting H.-J., Hingst Th., Schreiber E. Breakdown and high-energy electron vacuum emission of MIS-structures. *J. Phys. D: Appl. Phys.*, 1999, vol. 32, pp. 1963–1970. https://doi.org/10.1088/0022-3727/32/16/303

Поступила в редакцию 05.05.2024; одобрена после рецензирования 06.05.2025;
принята к публикации 15.05.2025; опубликована 29.08.2025

The article was submitted 05.05.2024; approved after reviewing 06.05.2025;
accepted for publication 15.05.2025; published 29.08.2025